Enhanced efficiency of CdS/P3HT hybrid solar cells via interfacial modification

SALİH YILMAZ

İSMAİL POLAT

MURAT TOMAKİN

AHMET ÜNVERDİ

EMİN BACAKSIZ

Research Article

Enhanced efficiency of CdS/P3HT hybrid solar cells via interfacial modification

Salih YILMAZ[1],* , **İsmail POLAT**[2] , **Murat TOMAKİN**[3] , **Ahmet ÜNVERDİ**[4],
Emin BACAKSIZ[5]
[1]Department of Materials Engineering, Faculty of Engineering, Adana Science and Technology University,
Adana, Turkey
[2]Department of Energy Systems Engineering, Faculty of Technology, Karadeniz Technical University,
Trabzon, Turkey
[3]Department of Physics, Faculty of Arts and Sciences, Recep Tayyip Erdoğan University, Rize, Turkey
[4]Department of Nanotechnology and Engineering Sciences, Graduate School of Natural and Applied Sciences,
Adana Science and Technology University, Adana, Turkey
[5]Department of Physics, Faculty of Sciences, Karadeniz Technical University, Trabzon, Turkey

Abstract: The present paper examines the effects of surface modification of CdS with diverse dyes on fabricated CdS-based hybrid solar cells. The X-ray diffraction results showed that CdS thin films had a hexagonal phase with a preferred orientation along the (101) plane. Scanning electron microscopy indicated that the CdS specimen was composed of a granular structure while a P3HT layer was formed from tiny grains. Band gaps of the CdS thin films and the P3HT layer were 2.45 eV and 1.98 eV, respectively. The absorption spectra showed that different dye loading caused an increase in the absorbance of CdS thin films in the wavelength range of 400–650 nm. The photoluminescence of the CdS/P3HT structure including various dyes was lower than that of the pristine one, implying that efficient charge separation was achieved upon surface modification. Current density–voltage curves showed that the ITO/CdS/N719/Ag hybrid solar cell exhibited the best overall efficiency of 0.082%, which can be attributed to improvements in both short circuit current density (J_{sc}) and open circuit voltage (V_{oc}). These enhancements can be attributed to the creation of better interfacial contact between CdS and P3HT layers after dye loading.

Key words: CdS thin films, spray pyrolysis, P3HT, dye effect, hybrid solar cell

1. Introduction

Recently, organic–inorganic hybrid solar cells have gained much attention owing to their low cost and easy growth on flexible substrates compared to their inorganic-based counterparts. They have also combined the beneficial properties of both types of material in a solar cell. As an organic semiconductor material, P3HT has good optical and electrical characteristics such as p-type conductivity, high absorption coefficient in the visible region ($>10^5$ cm^{-1}), high hole mobility, and good solution processability [1]. On the other hand, the inorganic CdS semiconductor has proven to be a wonderful material in opto-electronic devices due to its direct band gap of 2.42 eV, n-type conductivity, high electron mobility, good photosensitivity, and good stability. These properties make CdS a suitable photoactive material in hybrid solar cells [2]. CdS thin films are easily prepared by many methods on ITO-coated glass substrates such as pulsed laser deposition [3], close-space sublimation [4], chemical bath deposition [5], and spray pyrolysis [6]. Compared to the others, spray pyrolysis is a simple,

---

*Correspondence: slh_yilmaz@yahoo.com.tr

solution-based, and inexpensive method. Moreover, high quality CdS thin films with a low growth temperature can be readily produced by this route.

The number of reports on CdS/P3HT hybrid solar cells has increased recently due to the combining of the solution processability of P3HT and the high electron mobility of CdS. For instance, Yüksel et al. produced CdS thin films on ITO-coated glass slides and found the maximum power conversion efficiency (PCE) of 0.15% in the heterostructure of ITO/CdS/P3HT [7]. Kumar et al. fabricated CdS/P3HT hybrid solar cells and recorded the highest PCE score of 0.56% [8]. Yavuz et al. synthesized CdS thin films on ITO glass substrates to fabricate ITO/CdS/P3HT:PCBM/PEDOT:PSS/Ag hybrid solar cells and they reached a maximum efficiency value of 0.29% [9]. It is seen from these reported papers that PCE values of the fabricated CdS-based hybrid solar cells remain low because of incompatibility between CdS and P3HT layers. It is well known that interfacial modification has a positive effect on the performance of fabricated solar cells in terms of improving the charge separation efficiency at the interface of CdS/P3HT. This leads to a reduction in recombination of charges and thus the lifetime of carriers is elongated. Consequently, the performance of the hybrid solar cells is improved [10]. Although a number of papers were published on the surface modification of ZnO- [11–13] and TiO_2-based hybrid solar cells [14], works on CdS-based ones are very rare [15,16]. In the present paper, for the first time, we offer an interfacial modification of CdS/P3HT with four different dyes, which are organic dye (Eosin-Y), indoline dye (D205), and Ru-based complex dyes (N719 and N3). They are planned to be used to modify the physical and chemical properties of the surface of CdS in order to obtain additional photocurrent as well as more efficient electron injection [17]. Therefore, the compatibility between CdS and P3HT can be accomplished by dye absorption, which gives rise to an enhancement in the PCE value. First of all, CdS thin films are deposited on ITO-coated glass slides by spray pyrolysis and subsequently four different dyes are separately loaded on the surface of CdS. P3HT layers are then spin-coated on both ITO/CdS and ITO/CdS/dye heterostructures. To finalize the device, Ag paste is deposited on the top of the fabricated heterostructures.

2. Experimental procedure

2.1. Synthesis of CdS thin films

CdS thin films were produced by a spray pyrolysis technique on ITO glass slides cut to 1×1.25 cm^2. The ITO slides were cleaned with acetone, absolute ethanol, and deionized water in an ultrasonic bath for 10 min, in that order, and then air flow was used to dry the surface of the slides. In the production process of CdS thin films, $CdCl_2$ (0.05 M) and thiourea (CH_4N_2S) (0.1 M) salts with 0.1 M were employed as Cd^{2+} and S^{2-} sources, respectively. These salts were dissolved in deionized water to prepare the stock solution with a pH of 6.5. The prepared solution was sprayed onto the ITO glass slides with the help of compressed air at 400 °C for 10 min. The interval between the ITO glass slides and the nozzle was kept at 20 cm and the spray rate was maintained at 2 mL/min. To grow homogeneous CdS thin films, ITO slides on a substrate plate were also rotated at 10 rev/min. After the spraying process, CdS samples were quickly removed from the substrate plate via an Al_2O_3 ceramic plate in order to prevent the oxidization of the thin films. It was seen that the ITO-coated glass slides were well covered by CdS thin films and the adherence of the films to the slide surface was quite good.

2.2. Surface modification with diverse dyes

While 5 mM Eosin-Y dye was dissolved in acetone, absolute ethanol as a solvent was utilized to solve equimolar (0.5 mM) N3 or N719 dyes. On the other hand, D205 dye with a molarity of 0.3 mM was dissolved in a

mixture solution composed of acetonitrile and tert-butyl alcohol with a molar ratio of 1:1. CdS thin films were submerged in each solution including various dyes and were left in that solution for 24 h. After this procedure, it was seen that each one of the dye loadings on the surface of CdS thin films was not sufficient. Therefore, it was attempted to load the surface of the CdS thin films further with each dye by a spin-coating technique. The surface of the CdS thin films was loaded with Eosin-Y dye using a spin coater operating at a rotational speed of 1000 rpm. This process was applied to the surface of the CdS thin films 20 times over 1 min. On the other hand, the rotational speed, loading duration, and number of repetitions were fixed at 1000 rpm, 1 min, and 15 times for N3 dye; 1000 rpm, 1 min, and 10 times for N719 dye; and 1500 rpm, 1 min, and 10 times for D205 dye in order to obtain better dye absorption on the surface of the CdS thin films.

2.3. Fabrication of CdS-based hybrid solar cells

Commercial P3HT material of 20 mg/mL was dissolved in 2 mL of chlorobenzene solution and the prepared solution was spin coated on the surface of the produced structures, resulting in the fabricated heterostructures of ITO/CdS, ITO/CdS/Eosin-Y, ITO/CdS/D205, ITO/CdS/N719, and ITO/CdS/N3. The rotational speed of the device was adjusted to 1000 rpm and this process was performed five times over 1 min. Ag paste with a contact area of 0.008 cm^2 was used as back and front contacts and thus the CdS-based hybrid solar cells were finalized.

2.4. Characterization

The structural characterization of the CdS thin films was achieved through X-ray diffraction measurement (Rigaku SmartLab Unit) employing CuK$_\alpha$ radiation in the interval of 20° –60° with steps of 0.01° at room temperature. The surface morphology and elemental ingredients of the produced samples were examined by scanning electron microscopy (SEM, JEOL JSM 6610) and energy dispersive X-ray spectroscopy (EDS, Oxford Instruments). Optical transmittance and absorbance spectra of the samples were taken in the wavelength interval of 400–1000 nm by a UV-VIS spectrophotometer (SpectraMax M5). Photoluminescence (PL) analysis was carried out by Dongwoo Optron equipment operating via Xe lamp with a maximum power of 450 W at room temperature. PL measurements were realized using an excitation wavelength of 325 nm for CdS and a laser with an excitation wavelength of 532 nm for all other samples. Current density–voltage (J-V) characteristics of the fabricated CdS-based hybrid solar cells were measured using a source meter (Keithley 2401) under a solar simulator (AM 1.5 illumination) with a power output of 93 mW/cm^2.

3. Results and discussion

Figure 1 demonstrates the XRD data of CdS thin films grown on ITO-coated glass slides. It is seen that the CdS thin films exhibit a polycrystalline character with a hexagonal wurtzite phase (JCPDS card no: 41-1049). The diffraction phenomenon occurs at 24.66°, 26.56°, 28.20°, 36.64°, 43.72°, 47.82°, 51.92°, 52.72°, and 58.30° corresponding to the reflection planes of (100), (002), (101), (102), (110), (103), (112), (201), and (202). The (101) reflection plane is predominant in the pattern, indicating a preferred orientation along this plane. It is often seen from the published reports that CdS thin films prepared by spray pyrolysis grew along the (101) plane [18]. Besides CdS peaks, some peaks belonging to ITO-coated glass slides are observed in the pattern. a and c lattice constants are in turn determined through the (100) and (002) planes and their values are 0.414 nm and 0.671 nm, respectively. The crystalline size (D) of the CdS thin films is calculated employing the Scherrer formula and the D score is 27.3 nm.
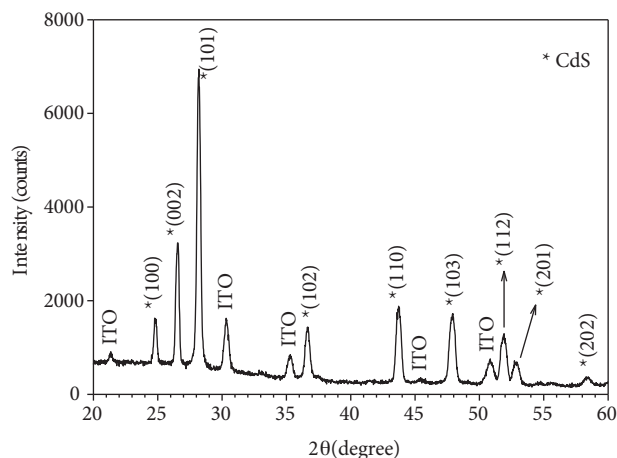
Figure 1. XRD pattern of CdS thin films grown on ITO-coated glass slides.

Figure 2a shows the top view of CdS thin films grown on ITO-coated glass slides. As seen, the CdS thin films are composed of granular grains. However, the grain distribution is not homogeneous throughout the surface, implying that there are tiny and large grains in the surface of the sample. It is also observed that the film surface has a compact morphology without any void. A 60° tilted SEM image is indicated in Figure 2b, proving that CdS thin films have an average thickness of 166 nm. Figure 2c shows a plain view photograph of the P3HT layer grown on the ITO/CdS structure. It appears that the P3HT layer includes grains that are too small to be observed. However, it is also seen that the P3HT layer is uniformly covered on the CdS thin films and its topography seems homogeneous. The film thickness of the P3HT layer is found to be about 238 nm from Figure 2d.

Figure 3 shows the EDS survey spectrum of CdS thin films grown on ITO-coated glass slides. The spectrum confirms the presence of Cd and S elements. It is seen from the inset of Figure 3 that the concentration of Cd is close to the amount of S in the CdS thin films, indicating that a stoichiometric CdS thin film is formed.

Figure 4a shows the optical transmittance data of CdS thin films grown on ITO-coated glass slides. It is notable that the CdS thin films display almost 80% transmittance in the wavelength region of 520–1000 nm, meaning that the sample produced has good transparency in the visible region, which is important for solar cell applications. The absorption edge shows a steep rise at nearly 500 nm, meaning that the crystal quality of the CdS thin films is good. Tauc's plot estimation is applied to derive the band gap value of the sample. Figure 4b shows that the band gap value of the CdS thin films is 2.45 eV, which is slightly higher than that of the bulk one. This could be due to the small deviation from stoichiometry of the film and the existence of some imperfections in the crystal structure.

The transmittance data of the P3HT layer grown on ITO-coated glass slides are depicted in Figure 5a. It is shown that the P3HT layer exhibits transmission over 90% in the wavelength interval of 650–1000 nm, implying very good transparency of the P3HT film. The band gap score of the P3HT layer is estimated by Tauc's method and found as 1.98 eV, as seen in Figure 5b, which is in good agreement with previous studies [19,20].

The absorption spectra of CdS/P3HT, CdS/Eosin-Y/P3HT, CdS/D205/P3HT, CdS/N719/P3HT, and CdS/N3/P3HT layers grown on ITO-coated glass slides are illustrated in Figure 6 to examine the effect of the modification with various dyes on the CdS surface. It is seen that the CdS/P3HT bilayer displays a wide
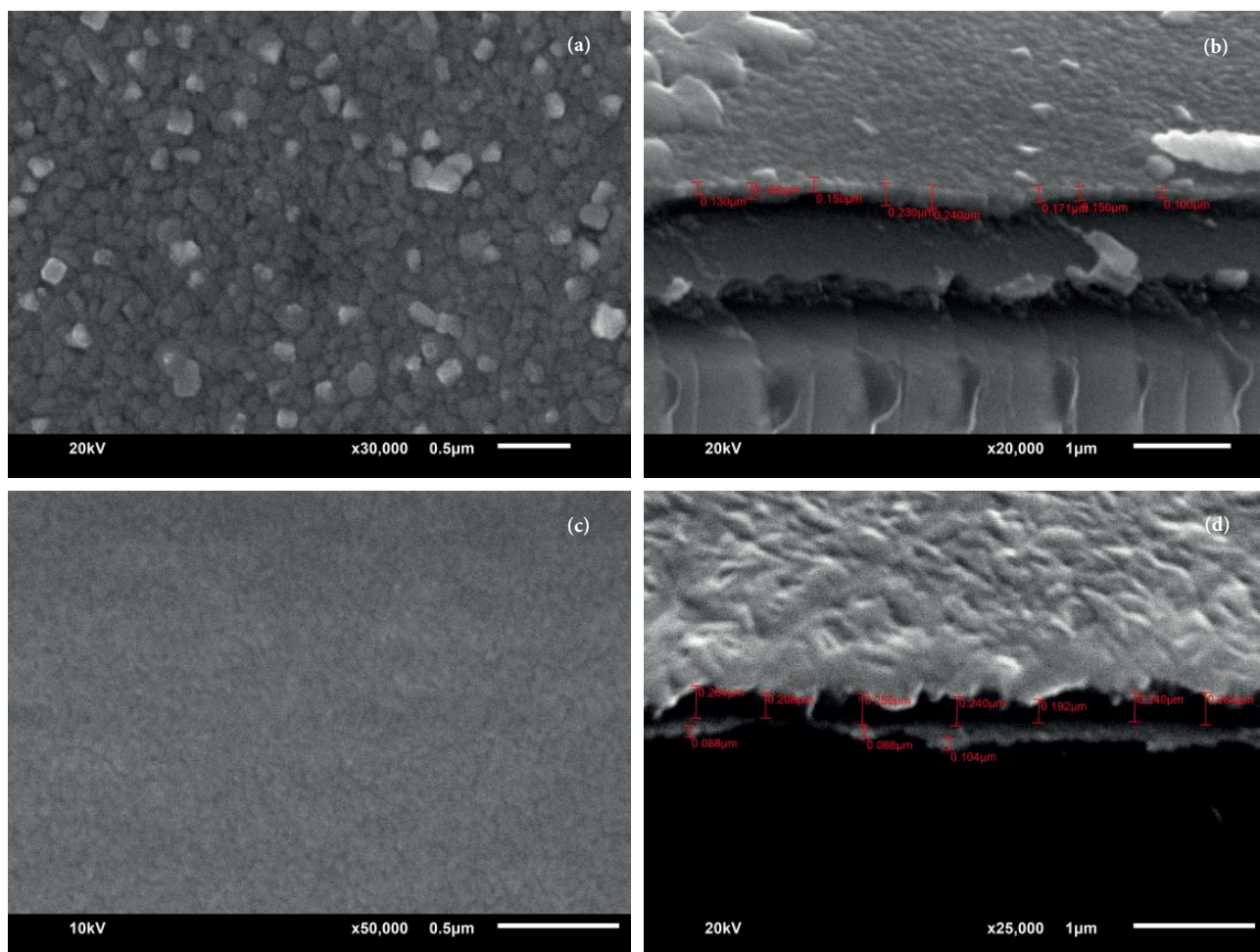
Figure 2. (a) Plain view and (b) 60°-tilted SEM images of CdS thin films grown on ITO-coated glass slides, (c) Top view and (d) 60°-tilted SEM pictures of P3HT layer grown on ITO/CdS thin films.
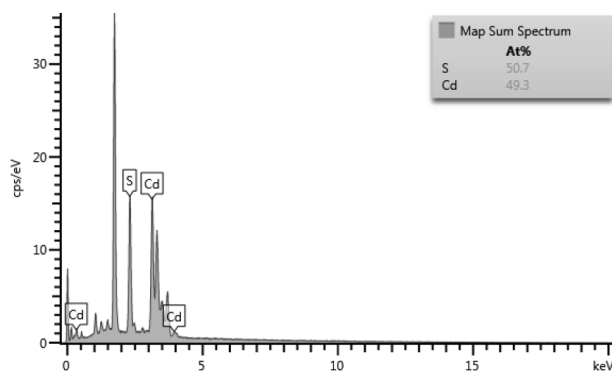

Figure 3. EDS survey spectrum of CdS thin films grown on ITO-coated glass slides.

absorption band between 400 nm and 650 nm with a maximum peak at 483 nm, which could be related to the vibronic transition of the P3HT molecule because of the strong interchain or intrachain $\pi - \pi$ interactions among polymer chains [21]. CdS/Eosin-Y/P3HT ternary films exhibit a similar spectrum to CdS/P3HT with
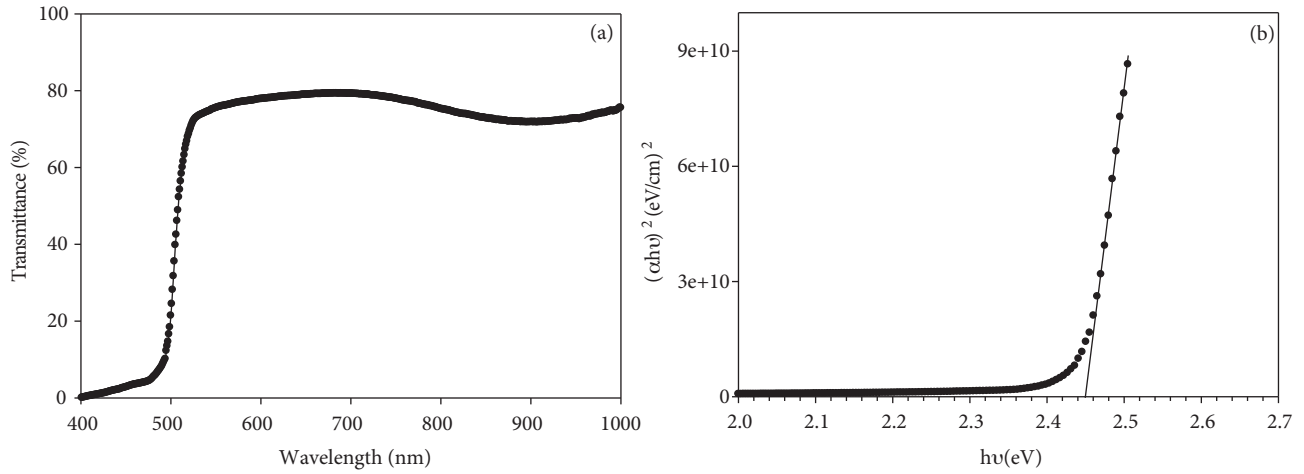
Figure 4. (a) Transmittance and (b) Tauc's curves of CdS thin films grown on ITO-coated glass slides.
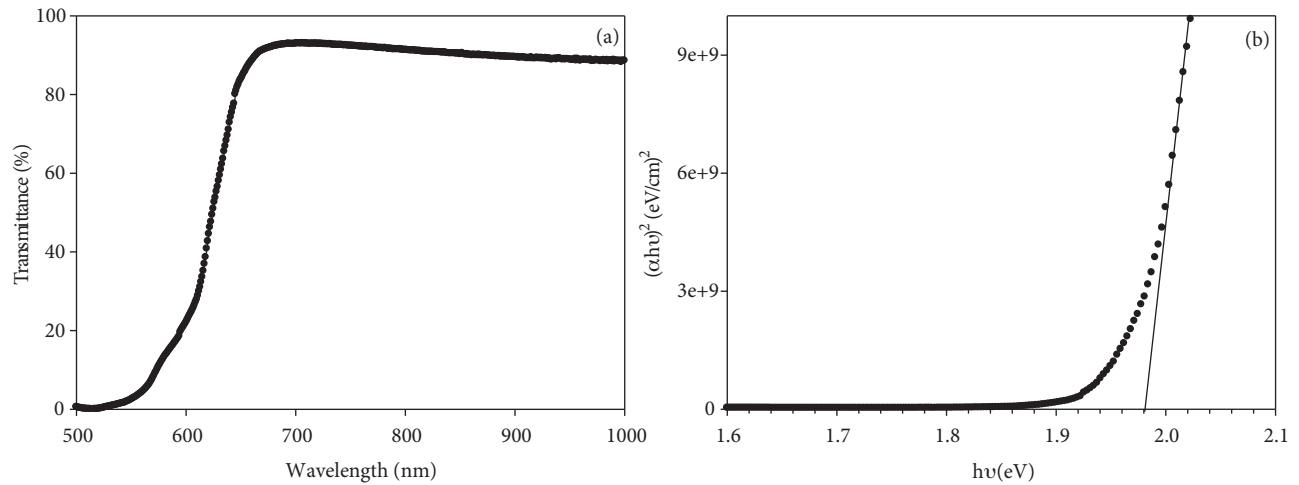

Figure 5. (a) Transmittance and (b) Tauc's curves of P3HT layer grown on ITO-coated glass slides.

the exceptions of peak intensity and peak shift, whereas CdS/P3HT layers including D205 dye have almost the same behavior as a pristine one (CdS/P3HT). On the other hand, totally different characters are obtained for CdS/N719/P3HT and CdS/N3/P3HT heterostructures relative to an unmodified one. This is due to the creation of strong $\pi - \pi$ interactions between the P3HT chain and N719 or N3 dyes, which leads to the spatial packing of P3HT and hence an enhancement in the intensity of the absorption spectrum is observed [16]. This increase in absorbance originates from dye loading, which provides a compatible interface between CdS and P3HT. However, after incorporation of Eosin-Y, N719, and N3 dyes at the interface of CdS/P3HT, a broadening in the light absorption spectrum towards the visible region is observed, confirming that dye loading is an efficient way of achieving the photon harvesting capability.

The defect structure of the samples is examined through room temperature PL analysis. Figure 7a shows the RTPL data of CdS thin films grown on ITO-coated glass slides. It is observed that the CdS thin films display two fundamental peaks, located at 503 nm and 680 nm. The first one belongs to the band gap emission of CdS (green region), which originates from the radiative recombination of excitons [22]. The
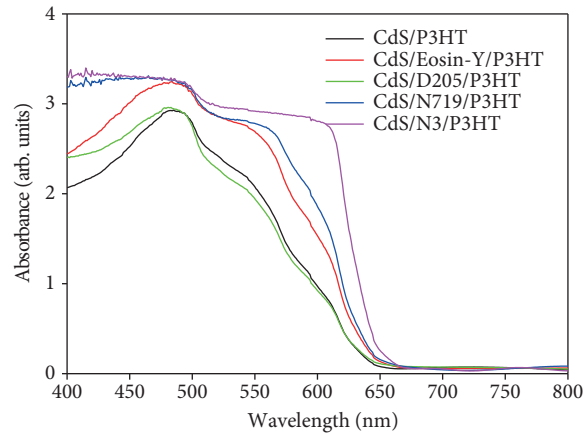
Figure 6. Absorption spectra of CdS/P3HT, CdS/Eosin-Y/P3HT, CdS/D205/P3HT, CdS/N719/P3HT, and CdS/N3/P3HT layers grown on ITO-coated glass slides.

second one, exhibiting an asymmetric structure ranging from 525 nm to 800 nm, can be ascribed to the deep level emission. This broad peak can be often attributed to point defects such as cadmium interstitial (I_{Cd}), sulfur vacancy (V_S), and cadmium vacancy (V_{Cd}) [23]. The RTPL curves of P3HT, CdS/P3HT, CdS/Eosin-Y/P3HT, CdS/D205/P3HT, CdS/N719/P3HT, and CdS/N3/P3HT layers grown on ITO-coated glass slides are shown in Figure 7b. It is worth mentioning that analogous spectral features are observed for all the heterostructures with an exception of peak intensity, implying that the PL data of P3HT dominate all the spectra. Compared to the unmodified bilayer (CdS/P3HT), after modification with various dyes of the CdS surface, PL intensity significantly quenches, indicating effective electron transfer from P3HT to CdS, leading to an efficient exciton dissociation at the interface of CdS/P3HT [15,24]. This means that a better interfacial compatibility is accomplished by surface modification, which is also consistent with the optical ab sorption conclusions.

The J-V curves of ITO/CdS/P3HT/Ag, ITO/CdS/Eosin-Y/P3HT/Ag, ITO/CdS/D205/P3HT/Ag, ITO/ CdS/N719/P3HT/Ag, and ITO/CdS/N3/P3HT/Ag hybrid solar cells measured under illuminated conditions
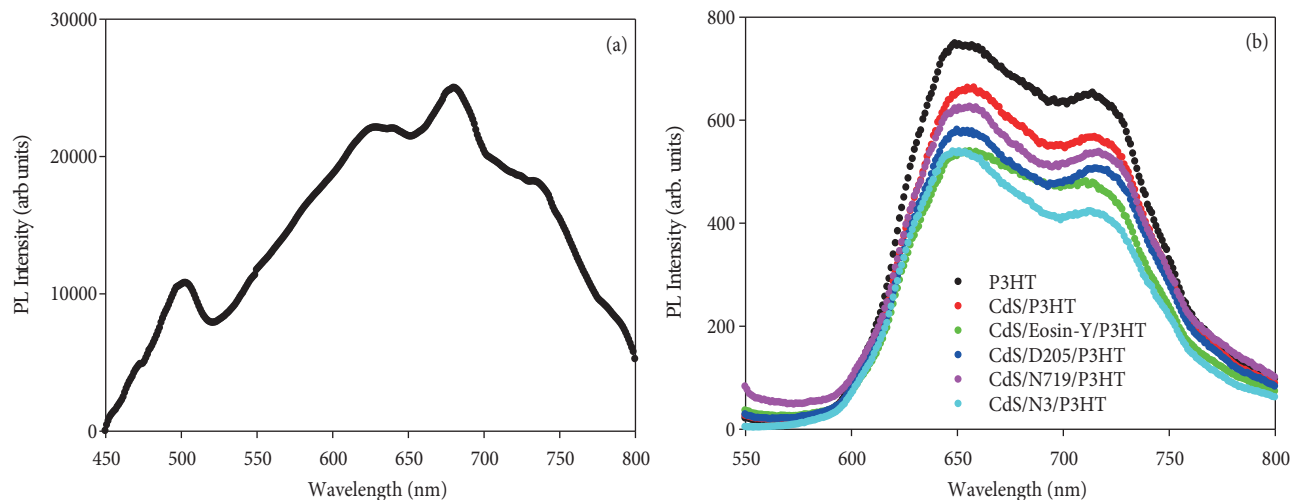

Figure 7. RTPL plot of (a) CdS thin films, (b) P3HT, CdS/P3HT, CdS/Eosin-Y/P3HT, CdS/D205/P3HT, CdS/N719/P3HT, and CdS/N3/P3HT layers grown on ITO-coated glass slides.

are represented in Figure 8 and key parameters of the devices are listed in the Table. It is remarkable that all the devices have a clear photovoltaic effect. In particular, it is notable that the CdS/P3HT cell demonstrates a J_{sc} of 0.30 mA/cm^2, a V_{oc} of 0.14 V, a fill factor (FF) of 0.33, and a power conversion efficiency (PCE, η) of 0.015%, which is low since hydrophilic CdS and P3HT surfaces give rise to a poor interfacial contact area [15]. It can be also seen from the PL data of CdS (Figure 6a) that CdS displays a defected structure, which is another reason for obtaining a low PCE [25]. Compared to the nonmodified hybrid solar cell, the CdS/Eosin-Y/P3HT one exhibits nearly the same J_{sc} and FF scores, whereas the V_{oc} value greatly improves from 0.14 V to 0.49 V. This leads to an overall conversion efficiency of 0.057%, which is an indication of improvement of almost four-fold. The reason for the increased V_{oc} is that surface treatment with Eosin-Y dye suppresses the charge recombination owing to the blocking of direct contact between CdS and P3HT, leading to a minimization of hole transfer from P3HT to CdS [11,26]. The cell including D205 modifier has a J_{sc} of 0.60 mA/cm^2, a V_{oc} of 0.23 V, a FF of 0.40, and a PCE of 0.059%, which are much higher than those of a pristine cell. This could be attributed to the improvement in the wettability of the CdS surface with D205 dye due to the interaction between the dye and water molecules, resulting in the formation of a hydrophobic surface [27]. The D205 molecule adsorbed on the surface of CdS that has a dipole moment contribution to the built-in voltage also induces an increment in the V_{oc} score [12]. On the other hand, the best efficiency of 0.082% is obtained for the CdS/N719/P3HT hybrid solar cell, indicating that N719 dye modification not only enhances J_{sc} but also improves V_{oc} compared with the unmodified cell. Although the J_{sc} value of the CdS/N3/P3HT cell does not change significantly, this cell displays the highest V_{oc} score of 0.69 V compared to the other devices. The cell performance is 0.080%. These enhancements in the efficiency of solar cells including Ru-based dyes of N719 and N3 could be due to improving electronic coupling between the absorbed N719/N3 dyes and CdS [16]. Similar results were also reported by Zhong et al. for CdS/P3HT and Lin et al. for TiO$_2$/P3HT hybrid solar cells upon modification with N719 and N3 dyes, respectively [14,15]. It can be concluded that the surface modification of CdS with Eosin-Y, D205, N719, and N3 dyes plays a crucial role to improve the photovoltaic efficiency of fabricated hybrid solar cells. The reasons for the increase in efficiency after dye loading can be summarized as follows: (i) the surface modification improves the light absorption efficiency as a result of obtaining a better P3HT chain alignment as shown by the absorption spectra (Figure 6) [17]; (ii) exciton separation efficiency at the interface of CdS/P3HT increases with surface treatment due to the enhanced interfacial compatibility between CdS and P3HT as discussed in the PL results (Figure 7b); and (iii) dye molecules behaving as a dipole trigger an interfacial electric field that promotes charge separation and hence prevention of back recombination at the interface of the CdS/P3HT bilayer is achieved [14].

Table. J_{sc}, V_{oc}, FF, and power conversion efficiencies (η) of ITO/CdS/P3HT/Ag, ITO/CdS/Eosin-Y/P3HT/Ag, ITO/CdS/D205/P3HT/Ag, ITO/CdS/N719/P3HT/Ag, and ITO/CdS/N3/P3HT/Ag hybrid solar cells.

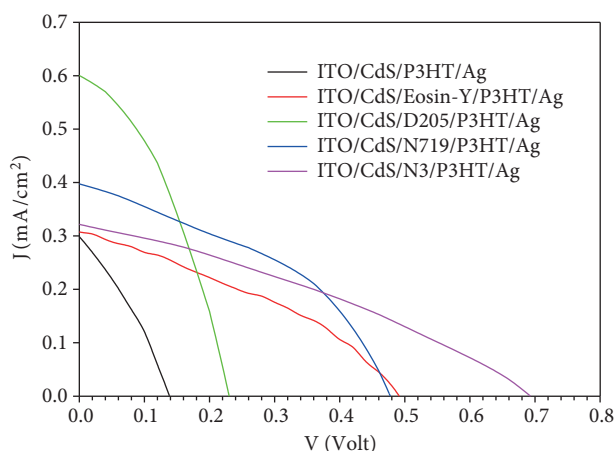| Device	J_{sc} (mA cm^{-2})	V_{oc} (V)	FF	η (%)
ITO/CdS/P3HT/Ag	0.30	0.14	0.33	0.015
ITO/CdS/Eosin-Y/P3HT/Ag	0.31	0.49	0.35	0.057
ITO/CdS/D205/P3HT/Ag	0.60	0.23	0.40	0.059
ITO/CdS/N719/P3HT/Ag	0.40	0.48	0.33	0.082
ITO/CdS/N3/P3HT/Ag	0.32	0.69	0.34	0.080

Figure 8. J-V curves of ITO/CdS/P3HT/Ag, ITO/CdS/Eosin-Y/P3HT/Ag, ITO/CdS/D205/P3HT/Ag, ITO/CdS/N719/P3HT/Ag, and ITO/CdS/N3/P3HT/Ag hybrid solar cells.

4. Conclusions

Spray pyrolysis was employed to prepare CdS thin films on ITO-coated glass slides. The XRD data confirmed the presence of a wurtzite structure in the CdS sample. SEM analysis depicted that homogeneous coverage was achieved for CdS and P3HT layers. The transmission data indicated that transparent CdS and P3HT films were formed. Tauc's estimation results demonstrated that CdS and P3HT films had band gaps of 2.45 eV and 1.98 eV, respectively. The absorbance results showed that dye loading increased the absorption capability of the CdS thin films, resulting in a better interface at CdS/P3HT. The PL data indicated that CdS thin films had a defect structure. Surface modification with dyes led to a decline in the intensity of PL, suggesting that charge separation efficiency improved. The J-V curves displayed an obvious PV effect and, compared to an unmodified one, CdS/P3HT hybrid solar cells including different dyes exhibited higher PCE values. It can be concluded that the surface treatment had a significant role in enhancing the PCE of the fabricated CdS-based hybrid solar cells.

Acknowledgment

References

[1] Cortina-Marrero, H. J.; Martinez-Alonso, C.; Hechavarria-Difur, L.; Hu, H. *Eur. Phys. J. Appl. Phys.* **2013**, *63*, 10201-10207.

[2] Jia, H.; He, W.; Zhang, Y.; Lei, Y.; Xiang, Y.; Zhang, S.; Zheng, Z. *New J. Chem.* **2013**, *37*, 3017-3023.

[3] Acharya, K. P.; Skuza, J. R.; Lukaszew, R. A.; Liyanage, C.; Ullrich, B. *J. Phys. Condens. Matter* **2007**, *19*, 196221-196225.

[4] Paudel, N. R.; Xiao, C.; Yan, Y. *J. Mater. Sci. Mater. Electron.* **2014**, *25*, 1991-1998.

[5] Jaber, A. Y.; Alamri, S. N.; Aida, M. S. *Thin Solid Films* **2012**, *520*, 3485-3489.

[6] Yılmaz, S.; Polat, İ.; Tomakin, M.; Küçükömeroğlu, T.; Töreli, S. B.; Bacaksız, E. *Appl. Phys. A* **2018**, *124*, 502-509.

[7] Yuksel, S. A.; Gunes, S.; Guney, H. Y. *Thin Solid Films* **2013**, *540*, 242-246.

[8] Kumar, N.; Dutta, V. J. *Colloid Interface Sci.* **2014**, *434*, 181-187.

[9] Yavuz, N.; Yuksel, S. A.; Karsli, A.; Gunes, S. *Sol. Energy Mater. Sol. Cells* **2013**, *116*, 224-230.

[10] Pei, J.; Hao, Y. Z.; Lv, H. J.; Sun, B.; Li, Y. P.; Guo, Z. M. *Chem. Phys. Lett.* **2016**, *644*, 127-131.

[11] Lim, E. L.; Yap, C. C.; Yahaya, M.; Salleh, M. M. *Semicond. Sci. Technol.* **2013**, *28*, 045009-045014.

[12] Ruankham, P.; Macaraig, L.; Sagawa, T.; Nakazumi, H.; Yoshikawa, S. *J. Phys. Chem. C* **2011**, *115*, 23809-23816.

[13] Bi, D.; Wu, F.; Qu, Q.; Yue, W.; Cui, Q.; Shen, W.; Chen, R.; Liu, C.; Qiu, Z.; Wang, M. *J. Phys. Chem. C* **2011**, *115*, 3745-3752.

[14] Lin, Y. Y.; Chu, T. H.; Li, S. S.; Chuang, C. H.; Chang, C. H.; Su, W. F.; Chang, C. P.; Chu, M. W.; Chen, C. W. *J. Am. Chem. Soc.* **2009**, *131*, 3644-3649.

[15] Zhong, M.; Yang, D.; Zhang, J.; Shi, J.; Wang, X.; Li, C. *Sol. Energy Mater. Sol. Cells* **2012**, *96*, 160-165.

16 Nan, Y. X.; Li, J. J.; Fu, W. F.; Qiu, W. M.; Zuo, L. J.; Pan, H. B.; Yan, Q. X.; Chen, X. Q.; Chen, H. Z. *Chinese J. Polym. Sci.* **2013**, *31*, 879-884.

[16] Zhong, P.; Que, W. X.; Zhang, J.; Yuan, Y.; Liao, Y. L.; Yin, X. T.; Kong, L. B.; Hu, X. *Sci. China-Phys. Mech. Astron.* **2014**, *57*, 1289-1298.

[17] Yılmaz, S.; Polat, İ.; Tomakin, M.; Töreli, S. B.; Küçükömeroğlu, T.; Bacaksız, E. *J. Mater. Sci. Mater. Electron.* **2018**, *29*, 14774-14782.

[18] Kron, R.; Lenes, M.; Hummelen, J. C.; Blom, P. W. M.; Boer, B. D. *Polym. Rev.* **2008**, *48*, 531-582.

[19] Dou, L.; Liu, Y.; Hong, Z.; Li, G.; Yang, Y. *Chem. Rev.* **2013**, *115*, 12633-12665.

[20] Kim, Y. J.; An, T. K.; Oh, S. J.; Chung, D. S.; Park, C. E. *APL Mater.* **2014**, *2*, 076108-076113.

[21] Lin, Y. J.; You, C. F.; Chang, H. C.; Liu, C. J.; Wu, C. A. *J. Lumin.* **2015**, *158*, 407-411.

[22] Yılmaz, S.; Töreli, S. B.; Polat, İ.; Olgar, M. A.; Tomakin, M.; Bacaksız, E. *Mater. Sci. Semicond. Process.* **2017**, *60*, 45-52.

[23] Jiang, X.; Chen, F.; Qiub, W.; Yan, Q.; Nan, Y.; Xu, H.; Yang, L.; Chen, H. *Sol. Energy Mater. Sol. Cells* **2010**, *94*, 2223-2229.

[24] Chen, F.; Qiu, W.; Chen, X.; Yang, L.; Jiang, X.; Wang, M.; Chen, H. *Sol. Energy* **2011**, *85*, 2122-2129.

[25] Thitima, R.; Patcharee, C.; Takashi, S.; Susumu, Y. *Solid-State Electron.* **2009**, *53*, 176-180.

[26] Ruankham, P.; Yoshikawa, S.; Sagawa, T. *Phys. Chem. Chem. Phys.* **2013**, *15*, 9516-9522.